Campanella *et al. Heritage Science* (2022) 10:79
https://doi.org/10.1186/s40494-022-00715-4

Heritage Science

RESEARCH ARTICLE Open Access

A green approach to clean iron stains from marble surfaces

Luigi Campanella[1*], Francesco Cardellicchio[2*], Emanuele Dell'Aglio[1], Rita Reale[1] and Anna Maria Salvi[2]

Abstract

In the field of cultural heritage restoration, the removal of iron corrosion stains is a difficult problem to deal with, especially in stone materials. Many studies in recent years have been aimed at finding simple and reliable methods using non-toxic chelating compounds. The search for natural non-toxic compounds is therefore of great relevance, especially in the conservation of cultural heritage, where the use of toxic chemical compounds often involves risks for the environment and human health. Following this trend, the purpose of this preliminary work was to verify the use of two proteins, Lactotransferrin (Ltf) and Ovotransferrin (Ovt), for the removal of iron-based stains on marble surfaces. The two proteins, whose high affinity for iron "in vivo" has been widely documented, were extracted from their natural matrices. The protein extracts were then immobilized using a common cellulose pulp. The poultices obtained were spread on the surfaces of artificially stained marble specimens and, after a set time, were easily removed. The effectiveness of the removal, visually evident, was detected by spectrocolorimetry and image analysis. The surface analyses, before and after the treatment, carried out by X-ray photoelectron spectroscopy (XPS), confirmed that both proteins have a selective and effective complexing capacity for the ferric ions of rust stains.

Keywords: Iron staining, Lactotransferrin, Ovotransferrin, XPS, Cultural heritage, Conservation

Introduction

Monument surfaces interact with the surrounding environment; the effects of these interactions evolve over time, depending on both the location and the characteristics of the constituting materials. The generation of stains, produced by iron corrosion phenomena, for example, can derive both from the oxidation of ferrous compounds existing in the stone, such as pyrite and siderite, and from the proximity of ferrous metals, which are oxidized due to air, humidity or acid rains [1–3]. Therefore, atmospheric pollutants, humidity, suspended particulate, biological components, are factors of great importance to the corrosion chemistry of metals and of carbonate stones. Examples of synergistic effects between chemical, physical, and biodeterioration factors are amply reported in the literature [4]. Specific chromatic alterations, occurring when metal parts, such as kingpins, brackets, nails, decorative elements, stabilization reinforcements, etc. are close to the carbonate stones, are certainly related to some aspects of the corrosion chemistry [5, 6].

In fact, it is well known how the combination of stone materials with some metals or alloys, like bronze statues on stone pedestals, promotes the formation of colored stains from corrosion products that affect the surface of the monuments, not only aesthetically, but also favoring or inhibiting specific biological activities [7]. XPS spectroscopic investigations on Roman monuments, holding bronzes or other copper alloys artifacts, have shown that in outdoor conditions the corrosion products, by the action of rainwater, drained off and migrated through the porous surface of the stone, forming stains of different colors and intensities [8, 9]. In these XPS analyses, copper compounds and mixed calcium/copper carbonates, associated with the

*Correspondence: luigi.campanella@uniroma1.it; f.cardellicchio@gmail.com

[1] Chemistry Department, University 'La Sapienza', Piazzale A. Moro 5, 00185 Rome, Italy
[2] Science Department, University of Basilicata, Via Dell'Ateneo Lucano 10, 85100 Potenza, Italy

stains were identified, as well as the presence of other elements (e.g. Pb, Zn), perhaps resulting from atmospheric contamination.

Similarly, the rust stains produced by corrosion of iron objects placed in proximity to marbles or carbonate stones were frequently observed on ancient and modern monuments [10, 11]: iron (III) compounds were easily identified by surface analysis techniques [12–14]. Furthermore, attention was paid to understanding the formation and growth of iron oxides on carbonate stones and to the influence of environmental and biological factors contributing to the weathering processes.

The detailed mechanism for rust formation is highly complex [11]; depending on the pH value, different compounds, all characterized by a brownish color, are formed. Typically, in the iron stains, lepidocrocite has been generally found which tends to transform itself over time into better-defined forms, such as goethite and hematite [15].

Iron stains can be removed from stone surfaces by chemical treatments. The methods involve the application of various compounds with complexing and reducing action, mixed on suitable supports. Generally, carboxylic acids have been the most used compounds in the cultural heritage sector, both for their lower aggressiveness towards artifacts and for their chelating capacity of iron.

One of the most used complexing agents has been the citrate [5, 16, 17], although other carboxylic acids, such as oxalic and tartaric acid, have also been tested. Other methods have involved the use of ethylenediaminetetraacetic acid (EDTA) [18] or the hexadentate binder N, N, N′, N′-tetrakis-(2-pyridylmethyl)ethylenediamine (TPEN) which has a high affinity for iron and a low affinity for calcium [1]. The various complexing agents have been used plain or in combination with reducing compounds, such as thiosulfate and sodium dithionite [16, 19]. Thioglycolic acid and ammonium thioglycolate have been applied in various treatments on carbonate stones [18]. Thioglycolate is presumably the most efficient compound for cleaning rust-stained marble [17, 18]: however, thioglycolic acid is a toxic compound and is therefore difficult to acquire and handle by conservators. Thioglycolic acid is a corrosive compound and can cause sensitization and allergic reactions when in contact with the skin [20]. EDTA, on the contrary, is a less toxic compound, also used as a food additive. However, it has a high affinity not only for iron but also for calcium; therefore its use on marble must be carefully evaluated. Agar gels, added with EDTA or citrate, have been used to remove metals from the surface: metal ions are selectively transported into the gel phase by complexation with EDTA or precipitation as hydroxide [21]. A review on the use of agar gel for cleaning artistic surfaces was presented by Sansonetti et al. [22].

More recently, attention has been paid to less toxic compounds such as natural iron chelants (e.g. amino acids) and to compounds used in medical therapy, such as deferoxamine and deferiprone [23]. Amino acids containing sulfhydryl groups, such as cysteine, or thioether groups such as methionine, mixed with sodium dithionite, have been used with good results [10, 11].

The research described here was carried out as part of the "SMART CITIES" project n°SCN_00520, funded by the Italian Ministry of University and Research. One of the objectives of the project has been the experimentation of increasingly ecological materials for sustainable restoration of cultural heritage, following the principles of "green chemistry". Within this context, this work regarded the development of a "green" cleaning procedure suitable for removing iron-based stains from marble surfaces of artistic-cultural interest, using non-toxic natural compounds, with respect both to the environment and human health. It is important to point out that every cleaning operation must guarantee not only the removal of alterations but also the conservation of authenticity of the historical and cultural heritage [24]. It is, therefore, necessary to identify materials and procedures that do not affect the characteristics of artifacts.

Therefore, the aim of this work was to verify the use of two proteins, Lactotransferrin (Ltf) and Ovotransferrin (Ovt), as innovative and non-toxic products for the cleaning of the stone surfaces from rust patches. For this purpose, in the laboratory samples of Carrara marble, exposed outdoor for 1 year in contact with metallic iron were tested.

The two proteins, both belonging to the transferrin's family and known for their high affinity for ferric ions in vivo [25–28], have been tested as substitutes for synthetic substances to remove iron oxides from marble surfaces, through the formation of stable complexes.

The ability of Ltf to bind iron can be understood with its three-dimensional (3D) structure. The molecule is folded into two homologous lobes (N- and C-lobes) with each lobe that can chelate a single Fe^{3+} ion. In the same way, the Ovt structure shows iron-binding sites are very similar to those reported for Ltf [29].

The two proteins were first extracted from their natural matrices and then mixed with the common cellulose pulp, completely wet. The poultices obtained have been spread on the surface of iron-stained marbles and carefully removed when their action was completed.

The ability of both immobilized proteins to remove the stains has been evaluated by a comparison of the spectrocolorimetric and XPS techniques. The comparison proved to be very useful for associating the variations in

color with the variation in the composition of the marble's surface before and after the treatment procedure. On the whole, the laboratory results have been very promising and made it possible to design new evaluation actions of the tested products for the conservation of marble surfaces.

Materials ad methods

Extraction procedures of Lactotransferrin and Ovotransferrin

Ltf (molecular weight 80-kDa) is a water-soluble multifunctional globular glycoprotein, which has two strong binding sites for Fe (III) ions. Ltf is present in bovine milk and colostrum at concentrations ranging between 0.2 and 1.5 mg/ml respectively and is the second most abundant protein in milk after the casein [30]. The extraction of Ltf was carried out from fresh commercial and whole milk, produced by the "Centrale del Latte in Rome". The procedure adopted is that described by Parkar et al. [30]. Briefly, 40 ml of milk were centrifuged for 10 min at 4000 rpm and 4 °C. After separation of the fats, 1 N HCl was added up to pH 4.6 to precipitate the casein. After centrifugation at 2000 rpm for 10 min, the supernatant, containing Ltf, was removed and stored at 4 °C.

1 N NaOH was added slowly with constant stirring to the supernatant till pH 6.0. The volume of solution was noted and an equal volume of 45% ammonium sulphate solution was added with constant magnetic stirring.

The sample was, then, added 1 N HCl slowly till pH 4.0 was reached, followed by the addition of 1 N NaOH till pH 8.0. At pH 8.0, an equal volume of 80% ammonium sulphate solution was added with constant magnetic stirring at 100 rpm. The sample was incubated at 4 °C overnight to precipitate lactoferrin. After centrifugation at 4000 rpm for 10 min at 4 °C, the precipitate obtained (about 80 mg) was resuspended in 20 ml of 0.01 M PBS (Phosphate Buffer Saline) at pH 7.4 and stored at 4 °C.

Ovt is the second most abundant protein in egg white after ovalbumin, (∼12–13% of the total egg proteins). The protein has a molecular weight of 76-kDa and contains about 700 amino acids. It is a powerful natural antimicrobial agent and the major binder of ferric iron [31].

The separation of Ovt from chicken eggs (Gold Ferioli, category A) was performed as described by Abeyrathne et al. [32]. An amount of egg white (150 ml) from 4 commercial fresh eggs was diluted with 300 mL of distilled water and homogenized manually. The pH was adjusted to 4.6 with 3 N HCl. The solution was centrifuged at 3400 rpm, for 30 min at 4 °C. The supernatant (about 300 ml) was added with 6 g of ammonium sulphate and 7.5 g of citric acid. The samples were kept overnight at 4 °C and centrifuged at 3400 rpm for 20 min at 4 °C. The precipitate was measured with a weighing balance; 12 g of precipitate were dissolved with 20 ml of distilled water, and then desalted using an ultrafiltration unit. After recovering the dialyzed solution, Ovt was precipitated from the solution by adding 0.4 g of ammonium sulfate and 0.5 g of citric acid. After storage overnight in the fridge at 4 °C, the samples were centrifuged at 3400 rpm for 20 min at 4 °C. The final precipitate, containing Ovt, was approximately 4.3 g (1.075 g per egg). About 400 mg were resuspended in 100 ml of 0.01 M PBS at pH 7.4, in order to have a solution with a concentration similar to that of Ltf.

Samples of Carrara marbles

The effectiveness of the two proteins was evaluated with tests performed on two Carrara marble samples ($100 \times 100 \times 20$ mm), called C and S; the stains were obtained by placing iron bars on the surface of the marbles and promoting corrosion through outdoor exposure for 1 year (terrace, Department of Chemistry, University of Rome). This type of exposure was chosen in order to obtain a mediated action between the various environmental conditions of temperature and rainfall over the four seasons. Oxidation was favored by rain and by the presence of atmospheric humidity and gave rise to the formation of stains (Fig. 1).

Carrara marble is mainly composed of $CaCO_3$ (∼97%,) with lower percentages of other compounds ($CaMg(CO_3)_2$ 1.76%, MgO 1.32%, SiO_2 0.71%). The marble's porosity usually is very low (from 0 to 1%), without a variability between marble types [33]. The ability to absorb water is however a very variable characteristic, depending on the structure of the material and from the environmental exposure conditions [34]. On the surface of the marble, the corrosion process leads to the formation of iron (III) oxides, identified, in some studies, as lepidocrocite [γ-FeO(OH)], which tends to transform over time into goethite [α-FeO(OH)] and hematite (α-Fe_2O_3) [15]. The concentration of iron oxides is greater in the portion in contact with the metallic element; on

Fig. 1 On the left, sample C of Carrara marble with superimposed iron bars: on the right, the stains produced

the surface of the marble, it is possible to observe the growth of a porous layer of iron oxide with a maximum thickness of a few tens of microns [14].

Cleaning procedures for removing iron stains

To immobilize the extracts protein, cellulose pulp was used; the pulp belongs to the category of inert supports and acts by the swelling of the cellulosic fibers (of different dimensions) due to imbibition of the various solvents (e.g. water, alcohol, etc.) or their mixtures [35].

Cellulose poultices are frequently used in stone treatment in order to remove soluble salts. They are easy to work with, have a neutral pH, high water absorption and plasticity, exhibit good adhesion to the substrate, and in most cases release low residues after clearance. Arbocel is a natural cellulose fiber composed of natural fibers and capable of retaining a quantity of water equal to 5 times its weight. Arbocel poultices contain water, which is readily given up to the substrate, leading to the rapid penetration of the moisture in the substrate.

For the applications reported in this work, the extracts of both proteins (20 mL in PBF buffer, pH 7.4) were mixed with white and de-resinated cellulose pulp (Arbocel BWW40), until obtaining a homogeneous mixture with the desired density and adhesion. The pH 7.4 was chosen to have a good chelating effect and, at the same time, to preserve the carbonate matrix of the marble.

The supported proteins were then applied over surfaces of two artificially stained Carrara marble specimens (C and S). Before the application, any possible dust residues adhering to the surface of the marble have been removed. The cellulose poultices were protected with a commercial polyethylene sheet to slow down the evaporation and thus prolong the cleaning action of the proteins. After 12 h, the polyethylene sheet and the cellulose pulp were removed, and the surfaces were cleaned with a cotton swab dipped in deionized water. Based on the experiences gained, the application time of 12 h was chosen to obtain the maximum cleaning action against iron stains and to avoid dehydration effects [36]. The treated surfaces were then monitored both photographically and with digital microscope observations.

Spectrocolorimetric analysis and digital microscopy of iron stains

The instrument used for the colorimetric analysis was a Konica Minolta CM-2600d spectrocolorimeter set with the following measurement parameters: spectral wavelength range between 360 and 740 nm, with a resolution of 10 nm; CIE standard illuminant D65; observer at 10° [37].

The color variations were measured with a portable digital microscope, Dino-Lite AM4815ZT, and the acquired micro-photos, before and after the treatment, were processed with the software for image analysis "Image J" [38]. Using the RGB (Red/Green/Blue) profiler plug-in for the color processing, it was possible to obtain histograms of the average RGB values of the individual pixels, useful for evaluating chromatic variations relating to the removal of iron oxides [39].

The reflectance curves were used to evaluate the removal of iron oxides. In each treated area, 12 measurements were made in order to calculate the average trend.

The normal reflectance spectra obtained by spectrocolorimetric measurements have been parameterized according to the Kubelka–Munk teory [40, 41], which provides one of the most useful transformations of the reflectance data.

This model, of an empirical nature, defines a remission function ($F(R_d) = K/S$) that relates the diffuse reflectance (Rd) of a homogeneously divided medium, not very absorbent and thick enough so as not to transmit light, to an absorption coefficient K and to a diffusion coefficient S of the medium. The Kubelka-Munkmodel theory has been widely used for the identification and quantification of iron oxides, especially in soils [42]. Since the original reflectance spectra or of the remission functions (K/S) result from the overlap of the absorption bands at different wavelengths, their resolution and interpretation are easier if the derivatives of the curves are obtained. The second derivative of the curve usually provides more information than the first derivative, because a band in the original spectrum, even if over imposed on other bands and not producing a true absorption maximum, always produces a minimum in the second derivative curve. Therefore in this work, the diffuse reflectance spectra have been transformed into the respective remission functions and subsequently, the parameters of the second derivative have been evaluated.

X-ray photoelectron spectroscopy (XPS)

The sampling for XPS analysis was performed by gently scraping the surface of the marble samples before and after treatment. The powder, collected from the examined areas, was firstly homogenized in an agate mortar and then pressed onto a double-sided copper tape, properly fixed on a steel sample holder, to be safely introduced in the analysis chamber of the spectrometer.

XPS spectra were acquired with a SPECS Phoibos 100- MCD5 spectrometer operating at 10 kV and 10 mA, in medium area (diameter = 2 mm) mode, using a MgKα (1253.6 eV) and AlKα (1486.6 eV) radiations. The pressure in the analysis chamber was less than 10^{-9} mbar during acquisition. Wide spectra were acquired in FAT (Fixed Analyser Transmission) or FRR

(Fixed Retarding Ratio) modes with a constant pass energy of 20 eV and channel widths of 1.0 eV.

High-resolution spectra were acquired in FAT mode, with a constant pass energy of 9 eV and channel widths of 0.1 eV, and were "curve-fitted" using the Googly program, which allows evaluating intrinsic and extrinsic features of XPS spectra [43, 44]. Peak areas and positions (Binding Energies, BE) as derived by the "curve-fitting" procedure were, respectively, normalized using proper sensitivity factors and referenced to the C1s aliphatic carbon set at 285.0 eV [45].

The assignments of the corresponding chemical groups and the relative percentage compositions were derived both from the analysis of standard compounds, acquired in the laboratory and from the NIST X-ray Photoelectron Spectroscopy Database [46].

Results and discussion

Treatment sequence of the samples

Figure 2 shows the sequence adopted to remove iron stains produced on two Carrara marble samples (C and S) after 1 year of outdoor exposure. The cellulose pulp, mixed with the two selected proteins, was applied on a portion of the surface for 12 h. To measure the color variations on marble surfaces, before and after the stains removal with the two protein extracts, spectrocolorimetric analysis and digital microscopy with "Image Analysis" were used.

Reflectance spectra and image analysis

One of the most obvious characteristics of iron oxides, hydroxides, and oxy-hydroxides is the variety of colors related to different types of electronic transitions. As a rule, iron oxides strongly absorb in the ultraviolet and blue spectral regions and reflect in the red and infrared regions. The absorption bands come from electronic transitions within the five 3d shells of the Fe (III) ion.

Significant differences can be observed between the individual oxides in the "warm" shades, ranging from the yellow of goethite to the purplish-red of some hematites. These absorption differences can allow distinguishing the different types of oxides. Figure 3 shows the trends of the reflectance curves for samples C and S before and after the treatment with Ltf and Ovt. As can be seen, there is a percentage increase of the reflectance in the post-treatment curves, especially in those areas of wavelengths characteristic of iron oxides (UV–Vis-near IR). The greater increase observed for sample S, treated with the poultice containing Ovt, confirms the more effective stain removal. This is also evident from the relative distance reduction from the blank reflectance curve, which corresponds to the color of the non-stained Carrara marble. The increase in percentage reflectance is more evident at low wavelengths in relation to the elimination of iron oxides which adsorb the incident radiation in this area: this is more evident with Ovt treatment.

The second derivative curve analysis of the original reflectance spectra or of the remission function (K/S) can be useful in order to obtain an indication about different

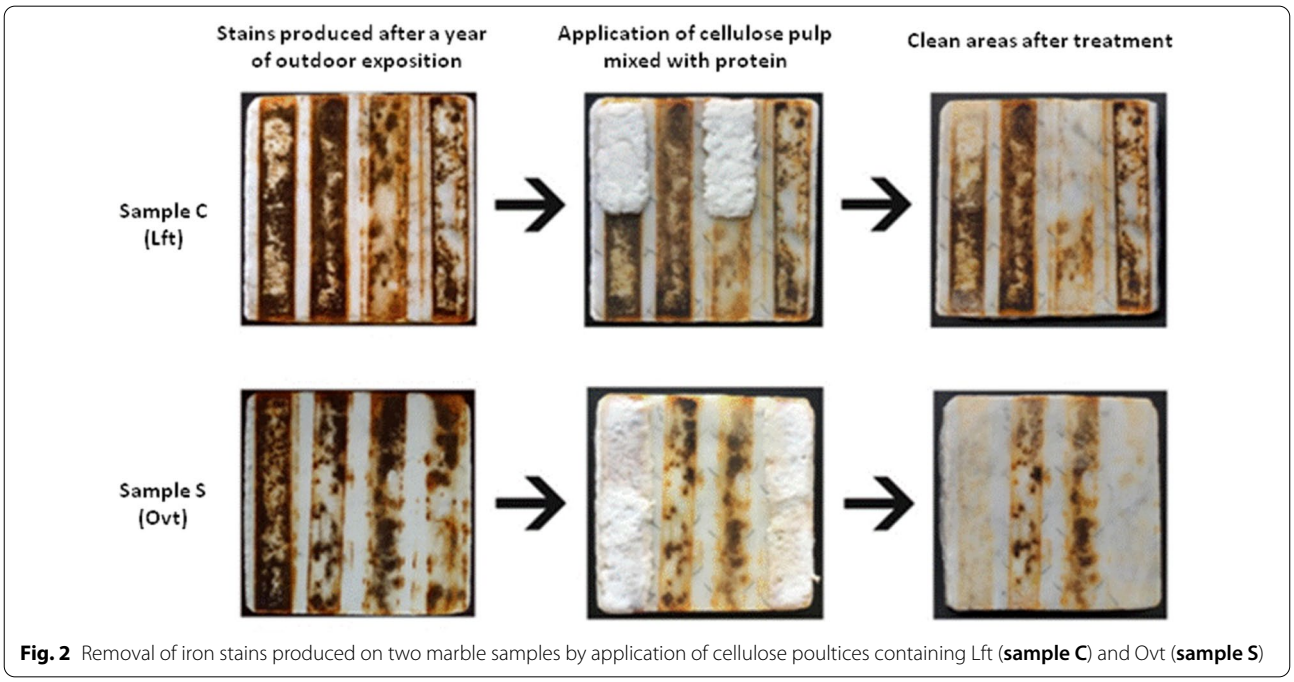

Fig. 2 Removal of iron stains produced on two marble samples by application of cellulose poultices containing Lft (**sample C**) and Ovt (**sample S**)

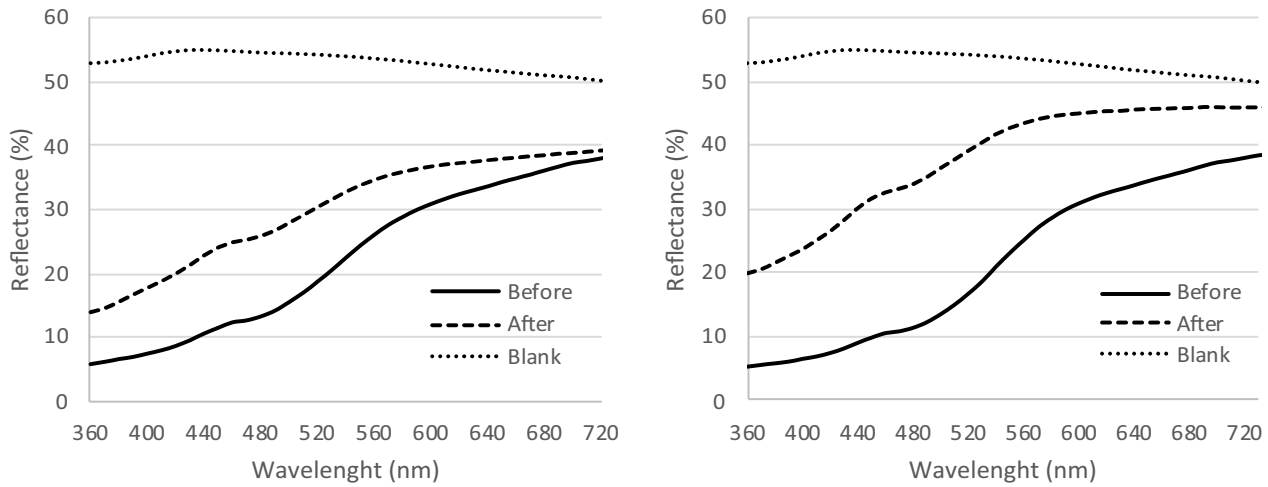

Fig. 3 Reflectance spectra for **samples C** (left) and **S** (right), before and after the removal of iron oxide, in relation to the blank curve

iron oxides present in the stained marbles and their crystalline properties [42, 47–49].

Figure 4 shows the trend of remission function and its second derivative, versus wavelengths (nm) for samples C and S before the treatment. Indicatively, the different K / S values between the two samples, especially at lower wavelengths, derive from the different distribution and concentration of the iron oxides on the surfaces of the two stained marbles.

In any case, in this work, the purpose was to identify not the concentrations but the peaks observable in the second derivative of the spectra for an evaluation of the type of oxides present.

Second derivative spectra generally show four/five bands between 370 and 730 nm, as the result of the combined overlap of the different adsorption bands of oxides. The bands with wavelengths greater than 520–580 nm are usually absent or weak (Fig. 4): these latter are instead indicative of the presence of hematite a are clearly separated from the more yellow iron oxides, such as goethite, which have peaks at about 425–480 nm [42]. The bands around the values of 420 and 480 nm are related,in fact, to electron transitions of iron oxides such as goethite (α-FeOOH) and ferrihydrite ($Fe_2O_3 \cdot 0.5H_2O$), although other oxides can contribute to absorption [42]. Although the distinction can only be indicative, from the analysis of second derivatives of the spectra in Fig. 4, it can be individuated the presence of hematite, of mixed phases of lepidocrocite/goethite and maghemite, the latter, characterized by the brown spots (Table 1).

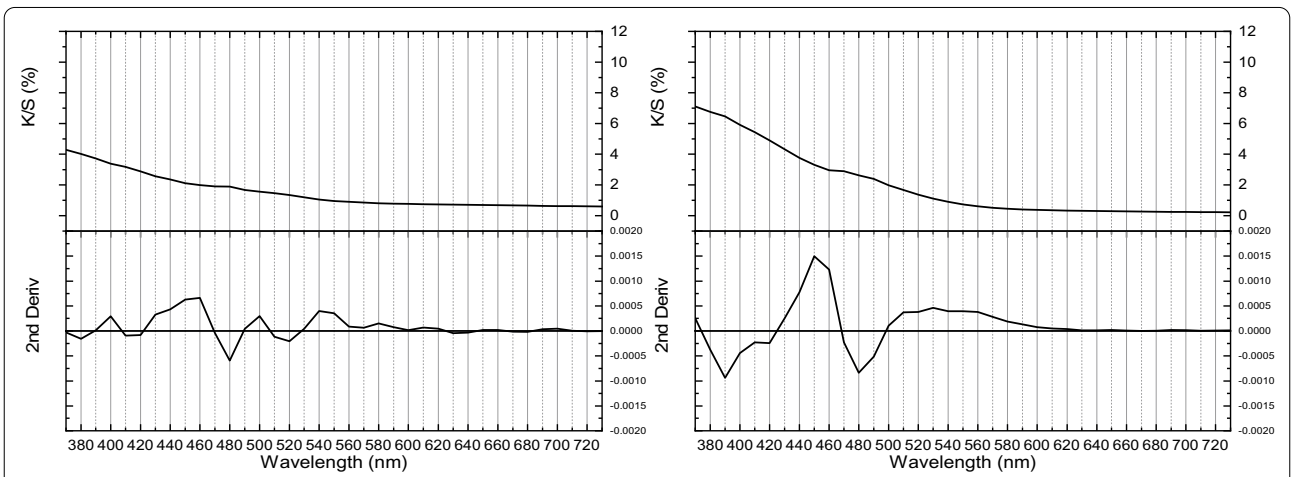

Fig. 4 Remission function (K/S coefficients) and its second derivative, versus wavelengths (nm): **samples C** (left), sample **S** (right) before the treatment

Digital microscopy, on the marble samples stained before and after the treatment, allowed the processing of images to extract meaningful information. The digital microphotographs acquired in several areas of analyzed samples (Fig. 5), have been processed by RGB color analysis, before and after the removal of iron stains with the Ltf and Ovt proteins. RGB analysis allowed us to represent the analyzed areas with histograms, Fig. 6(a, b), from which the results obtained from the application of the two proteins are evident.

Table 1 Absorption bands based on 2nd derivatives of Fig. 4

Wavelength (nm)						
Samples	**Ferrihydrite/Lepidocrocite/ Goethite**	**Ferrihydrite/Maghemite/Hematite/ Goethite/Lepidocrocite**		**Hematite**		**Maghemite**
C	380	410	480	520	570	–
S	390	420	480	520	560	620 (w)

(w) weak peak

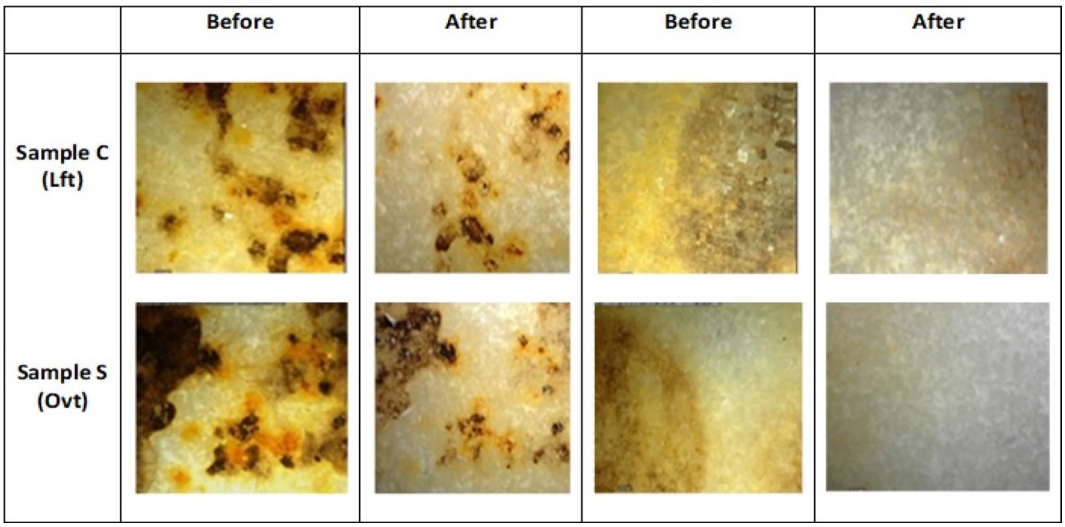

Fig. 5 Images of two areas of **samples C** (Ltf) and **S** (Ovt), acquired by digital microscopy before and after the treatment with the two proteins (magnification 75x)

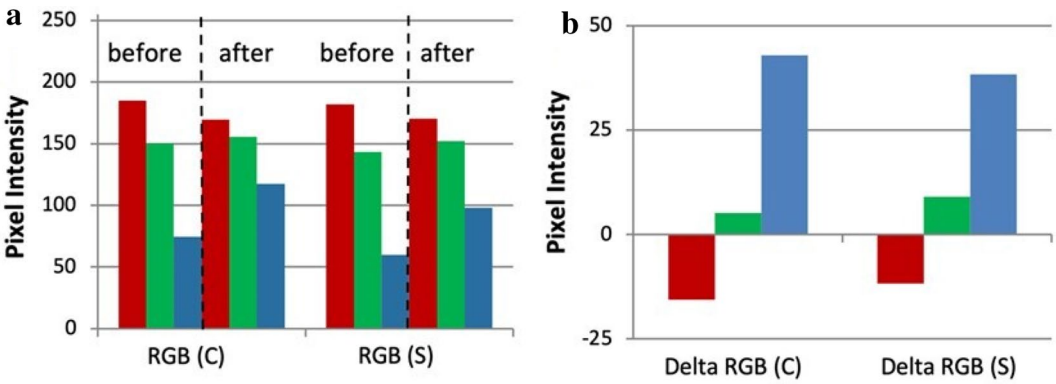

Fig. 6 **a** RGB averaged histograms of samples C (Ltf) and S (Ovt), before and after the treatment with the two proteins and **b** the relative difference (delta RGB)

In both cases, after the treatment, the observed Red decrease and the Green and Blue increase, indicate the color-changing toward the "white" of the not-stained marble. The color change towards white, as also observed in Fig. 3, is a result of a reflectance increase in the whole visible spectrum. The decrease of red and the increase of green and blue confirm the removal of the iron oxides, that absorb the green and blue wavelengths.

XPS analysis of standard iron compounds

Based on the XPS analysis of standard compounds reported in the literature, Fig. 7a shows how different peak shapes are associated with various oxidation states of iron oxides [50]. Figure 7b shows the detailed Fe2p region of standard iron (III) oxide (Sigma-Aldrich), curve-fitted with Googly program. The curve fitted Fe2p region shows the $2p_{3/2}$ and $2p_{1/2}$ positions (Binding Energies, eV), their broadening due to multiplet splitting (MS), and the presence of shake up (SU) satellites, all characteristic of the Fe^{3+} profile. From the combined analysis via curve-fitting of the Fe2p and O1s detailed regions, the obtained XPS results were those corresponding stoichiometrically to hydrated hematite, $Fe_2O_3 \cdot H_2O$.

The acquisition of this reference spectrum proved useful for subsequent analysis of the real samples, consisting of powders gently scraped from the surface of the marbles, under study. In fact, all XPS spectra of rusted marbles showed the typical Fe2p shape of iron (III) oxides and were all curve-fitted by referring to Fig. 7b.

XPS analysis of marble surfaces

The surface areas of two Carrara marbles, from which powders were collected for XPS analysis, are indicated in Fig. 8. As can be seen, the sampled surface area before and after the treatment was the same for the two marble specimens; for sample S, the sampling of the surface before treatment was carried out from another untreated area (area BO, Fig. 8) to verify the variability of the XPS results as a function of the area chosen for sampling. The powders taken from lateral sections not stained of the marbles were analyzed first and indicated as blank marble C (BC) and blank marble S (BS).

Comparing the XPS wide spectra of the two blank samples, BC and BS in Fig. 9 (upper), no substantial differences were noted in their characterization since the spectra were almost perfectly overlapped. Figure 9 (lower) and Table 2 respectively show the C1s, Ca2p, O1s curve-fitted regions related to sample BS and the results for the whole set of detailed regions, obtained following a well-established curve-fitting procedure adopted for all samples in this study [43, 44]. This procedure allows estimating surface composition by assigning chemical states (corrected BEs) and relative intensities to each peak resolved by curve-fitting (normalized areas). The procedure also allows performing the mass balance, taking into account the stoichiometric coefficients of each chemical group in the given compound, in the limits of XPS technique accuracy (±10%) [45]. In Fig. 10 the wide

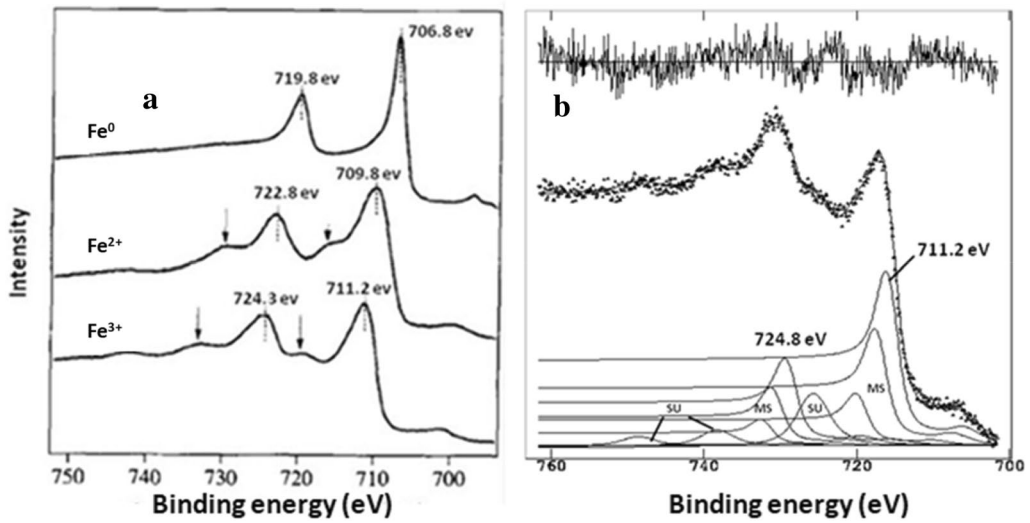

Fig. 7 **a** Superimposed Fe2p spectral shape of iron standard from Graat et al. [50]; **b** XPS Fe2p spectra of powdered Fe_2O_3 compound

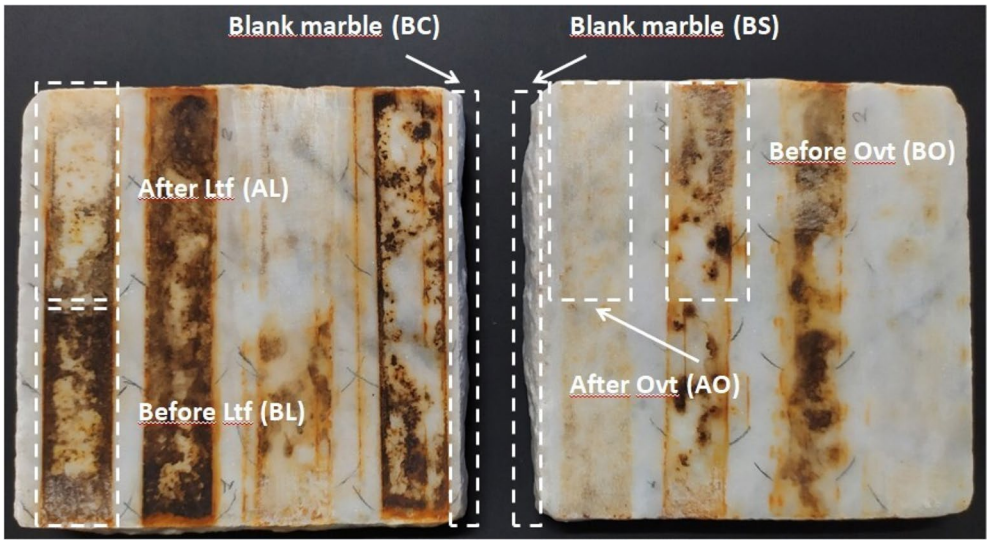

Fig. 8 Sampling areas (**dashed**) on Carrara marbles for XPS analysis; areas BC and BS: blank marble (**along the sample thickness**); areas BL and BO sampled before cleaning treatments; areas AL and AO sampled after treatment with the proteins (Lft and Ovt respectively)

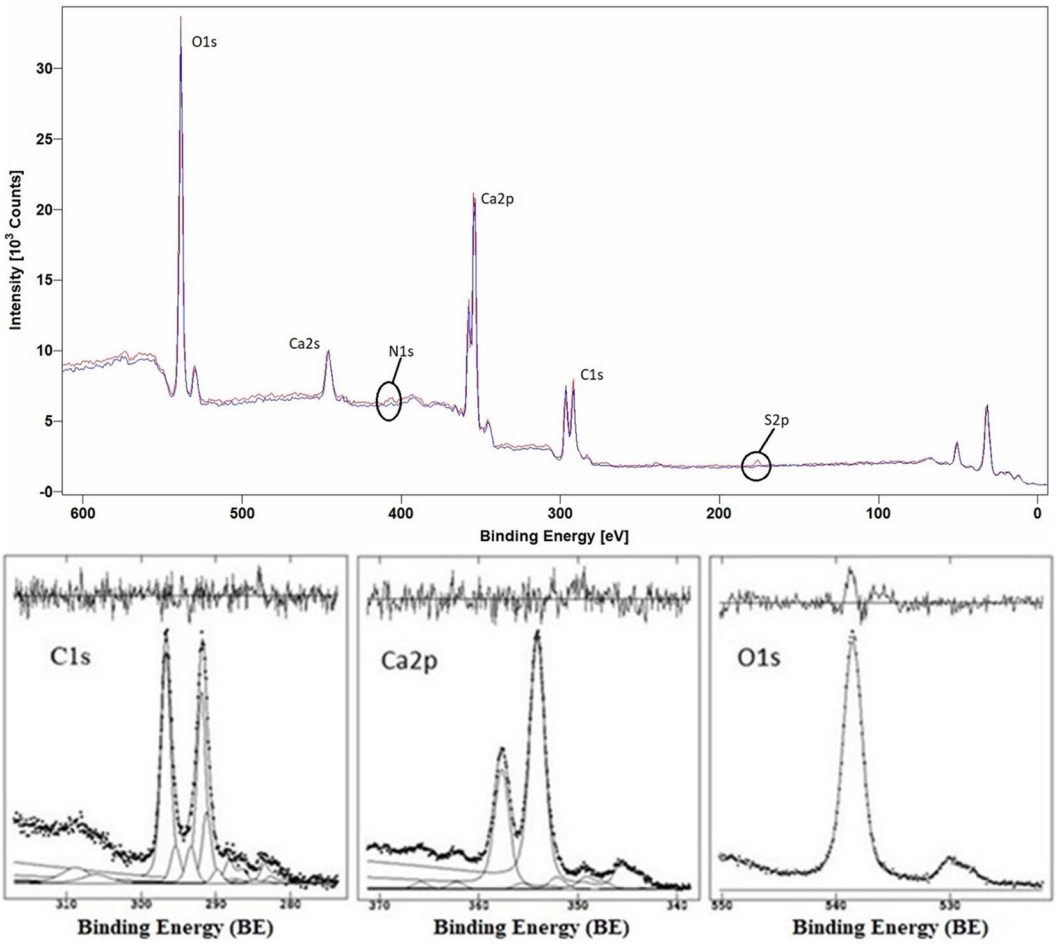

Fig.9 **Upper**, comparison of wide spectra: sample BC (red) – sample BS (blue); **Lower**, C1s, Ca2p and O1s curve-fitted regions for BS sample

Table 2 XPS curve-fitted data of the detailed regions of sample BS (Fig. 9)

Element/orbital	Corrected BE (eV ± 0.2 eV)	Normalized Area	Assignments (from NIST database, literature data and standard analyses)
C1s	282.8	3393	C–C aromatics
	284.3		
	285.0	7576	C–C aliphatics
	286.4	1454	C–O–C, C-N, C–OH, *ϕ-OH
	288.5	1483	*ϕ –CO–O, -CO-NH_2
	289.7	9158	CO_3^{2-}
S2p	168.6	188	S linked to an aromatic ring/ SO_4^{2-}/ SO_3^{2-}
O1s	531.6	30,157	●
Ca2p	345.1	462	Ca, CaO
	347.2	9137	$CaCO_3$

(●) O1s: total area accounts for all the oxygenated species, taking into account the stoichiometric coefficients of each chemical group in the given compound, in the limits of XPS accuracy (± 10%) [45]

Φ = aryl group

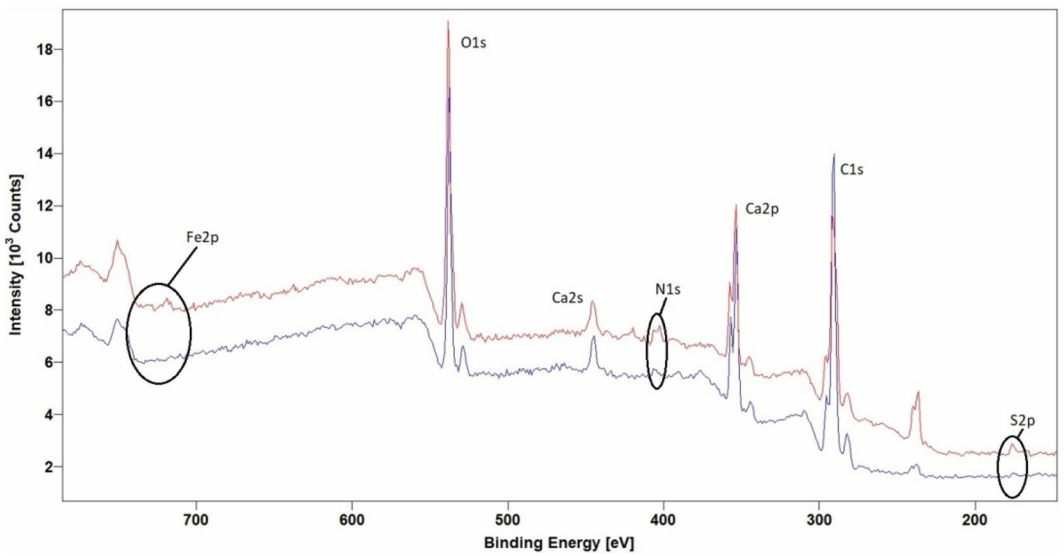

Fig. 10 Comparison of wide spectra of samples BO (**orange**) and AO (**blue**) before and after cleaning with Ovt

spectra of the samples taken from the BO and AO areas are shown: as can be seen, after the treatment with Ovt the iron signal disappears.

The XPS spectra of the powders taken from the various sampling areas outlined in Fig. 8 were processed by curve-fitting. The areas of the various peaks identified were then normalized and converted into percentage atomic composition (At%). The results for blank samples (BC and BS) and surfaces, before (BL and BO) and after (AL and AO) the cleaning treatment with Ltf and Ovt, are summarized in the pie charts of Fig. 11.

The results from blank samples confirm their comparable composition both for the main and minor constituents as shown in the pie charts of Fig. 11. In fact, the percentages of calcium carbonate and carbonaceous constituents (C–C group) were for the two blank marble samples: BC: CaCO3 36.0%, C–C 49.6%; BS, CaCO3 38.6%, C–C 46.3%. The non-negligible percentage of the carbonaceous components in the surfaces of non-rusted marbles was certainly related to the deposition of contaminants deriving by the city atmosphere during the 1-year exposure outdoor.

As shown by the number of peaks composing the carbon C1s signal, listed in Table 2, the blank surface of marbles is covered by carbonaceous contaminants, mainly consisting of aliphatic chains containing oxygen

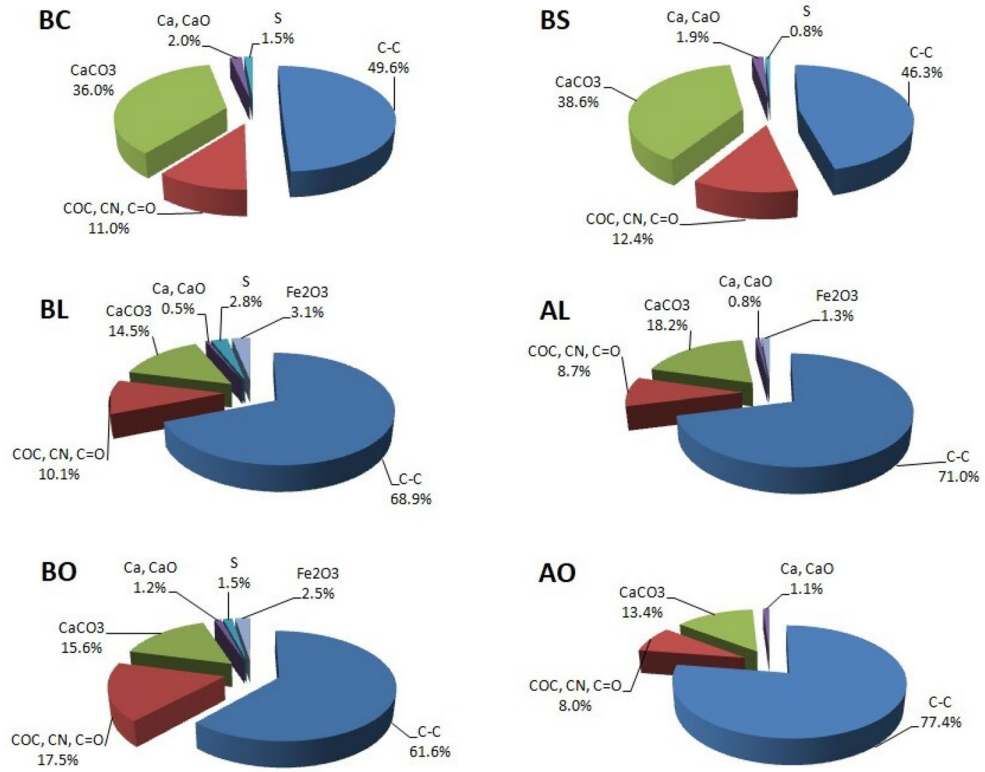

Fig. 11 The graphic comparison of curve-fitting results for blank samples (**BC** and **BS**), rusted marbles before (**BL** and **BO**) and after (**AL** and **AO**) cleaning with Ltf and Ovt. Note: C–C includes both organic and aliphatic carbon

and nitrogen groups. Additional unspecified adsorbed compounds are grouped as organic carbons typical of compounds such as polycyclic aromatic hydrocarbons, etc. [46, 51, 52].

Their co-presence, often found on monument surfaces [53] long exposed to atmospheric pollutants, contributes to the formation of the characteristic 'patina'. Here the term "*patina*" indicates, without discrimination, all the sequential layers, of both biotic and abiotic origin, possibly deposited over the "*noble patina*", formed over the underlying carbonate stone and eventually protective against the progressive erosion due to acidic rain and aggressive atmospheric components [54, 55]. The "*noble patina*" of an artifact is the slow deposit on the ancient surfaces that deserves to be preserved as it represents the testimony of the time that has passed.

By comparing the detailed spectra of the two samples sets (BL-AL) and (BO-AO) and the curve-fitting results reported in the corresponding pie charts of Fig. 11, the cleaning effects can be highlighted: after treatment with both proteins, in fact, the stoichiometry of $CaCO_3$ remains unaffected, while a reduction of iron and sulfur content and a relative increase of the carbonaceous components, more evident after treatment with Ovt, are observed. This increase could be attributed to the eventual release of other interfering compounds present in protein extracts. It is important to note that the values of the At% of iron (III) oxide decreased from 3.1% to 1.3% with Ltf treatment, and from 2.5% to not determinable with Ovt treatment, demonstrating that both proteins have an ability to clean iron stains. The effect of Ovt treatment is evident also in Fig. 10, where it is noted that the iron signal in the wide spectrum is no longer evident after treatment.

A further confirmation of the action of the two proteins can be obtained from the calculation of the Fe / Ca ratio which decreases from 0.20 to 0.07 after treatment with Ltf and from 0.20 to 0 after treatment with Ovt. The decrease in the ratio is linked to the elimination of iron, while the carbonate matrix of the marble is not affected by the treatment.

Due to the presence of iron compounds, the stained marbles were more contaminated than blank marble's surface, as evidenced by At% values in the relevant pie charts, where an increase of aliphatic and aromatic carbons is also observed. It is probable that during the corrosion process, various contaminants (for example atmospheric particulate) can be incorporated into the

rust stains [56], making it more difficult for the iron to bond with the chelating proteins and therefore its complete removal with single cleaning action. Therefore, the overall cleaning efficacy, monitored after a single treatment, clearly depends on the conditions under which the rust deposits form on surfaces and from the type of the associated contaminants.

The results obtained highlight the usefulness of the combined use of the two analytical techniques, which made it possible to correlate the color of the surface with its composition, providing information on the effectiveness of the treatment procedure for a single application. The two chelating proteins (Ltf and Ovt), supported in the cellulose pulp, have proved highly selective to solubilize iron in rusty marbles, without affecting the $CaCO_3$ substrate, whose integrity is confirmed by the At % values calculated after curve-fitting of XPS regions, as reported on the pie-charts (Fig. 11). The results of Fig. 11 show that Ovt is more effective than Ltf in the reduction of iron on the treated surfaces; after application of the cellulose pulp, impurities of proteins, resulting from the extraction process, can be released on surfaces, thus reducing iron XPS signals within the sampled powder [57].

In this sense, it is necessary to further improve the extraction method of two proteins from raw materials (eg milk and eggs) and to check for any other extracted compounds. Furthermore, the optimization of the procedures would allow to reduce the times and increase the extraction yield, given the costs of the two purified proteins on the market.

The results so far obtained also indicate how the surface *patina* induced by iron corrosion, contributes to the surface alteration of stone artifacts. In fact, several works have shown that the presence of iron oxides on carbonate stones is associated with the absorption of other components, such as biological components and carbonaceous particulate, all contributing to the alteration process.

Cleaning methods reported in the literature try to solve this complex problem with various strategies including the choice of chelants mixtures, the addition of redox components to control iron redox state and removing other organic/inorganic pollutants [1, 5, 11].

Within the National "Smart Cities" project, further multidisciplinary researches are underway on innovative cleaning methodologies, in order to eliminate, at the same time, rust and the associated pollutants in bioactive forms, present in real samples exposed to the external environment. In particular, iron-chelating compounds, such as glutathione and deferiprone, are also being evaluated on marbles comparing Fe/Ca ratio of the surface pre and post-treatment, as the best indicator of their performance [58, 59].

In this context, given the reported variations of Fe/Ca ratios and colors, respectively deducible from the XPS pie-charts and the elaboration of colorimetric images, the choice of natural Ltf and Ovt transferrins for the chelation of iron and their solvation in the neutral aqueous cellulose pulp, appears to be a promising way for cleaning artifacts of cultural interest.

Based on the obtained results, it is possible to foresee subsequent applications to remove rust patches still present on marble surfaces, after the first application. It is also important to underline the role of cellulose pulp in the mechanical removal of surface contaminants associated with iron oxides, and the possible action of the two transferrins studied, given their antimicrobial activity, in the control of biodeterioration without affecting the calcareous substrate [60, 61]. All these factors support the proposed research as a "green method" with a lower environmental impact, which ensures safety, non-aggressiveness for the treated matrices, and cleaning effectiveness.

Conclusions

The use of immobilized Ltf and Ovt has proved an effective technique for eliminating rust stains from marble artifacts, offering secure advantages and perspectives in the conservation of Cultural Heritage.

Firstly, the advantage found in the use of these two proteins, as an alternative to traditional chemical cleaning methods, was that of obtaining highly selective and non-invasive chelation of ferric ions. In fact, these chelating proteins act only on target compounds, without attacking other matrices, such as calcium carbonate.

Secondly, the immobilization system used is able to influence the degree of effectiveness in cleaning obtained, through a good capacity of retaining water, good maintenance of the contact time, and, finally, facilitating the mechanical removal of undifferentiated "*patina*", which contributes to altering the surfaces of marbles. From these points of view, the innovative value of the developed methodology, which can be adapted according to the required needs, reflecting the criteria of minimum intervention, must be emphasized. Another further advantage is represented by the "green" aspect of the methodology, which proves not only safe for the artifacts but also for the environment and for operators in the cultural heritage sector.

Acknowledgements

The Authors thanks the support of the Smart Cities National (SCN 00520) project "Product and process innovation for the maintenance, conservation and sustainable planned restoration of cultural heritage". The Italian Ministry of Education, Universities and Research, D.D. n. 428, 2014. Thanks are due to Dr. Fausto Langerame for his valuable contribution to the XPS analyses.

Author contributions
Conceived and designed experiment: LC and AMS. Perfomed the analysis: FC, EDA and RR. Analysis of data: LC, FC, EDA, RR and AMS. Wrote and revised the paper: LC, FC and AMS. The paper was approved by all authors. All authors read and approved the final manuscript.

Funding
Not applicable.

Availability of data and materials
All data analyzed during this study are included in this published article. Raw data (including spectra) are available from the corresponding authors on reasonable request.

Declarations

Competing interests
The authors declare that they have no competing interests.

Received: 15 December 2021 Accepted: 15 May 2022
Published online: 07 June 2022

References

1. Cushman M, Wolbers R. A new approach to cleaning iron stained marble surfaces. WAAC Newslet. 2007;29(2):23–8.
2. Macchia A, Sammartino MP, Tabasso ML. A new method to remove copper corrosion stains from stone surfaces. J Archaeol Sci. 2011;38:1300–7. https://doi.org/10.1016/j.jas.2011.01.005.
3. Bams V, Dewaele S. Staining of white marble. Mater Charact. 2007;58:1052–62. https://doi.org/10.1016/J.MATCHAR.2007.05.004.
4. Ciferri O. The role of microorganisms in the degradation of cultural heritage. Stud Conserv. 2002;47(1):35–45.
5. Matero FG, Tagle AA. Cleaning, iron stain removal and surface repair of architectural marble and crystalline limestone: the metropolitan club. J Am Inst Conserv. 1995;34(1):49–68. https://doi.org/10.2307/3179435.
6. Johansson LG. Synergistic effects of air pollutants on the atmospheric corrosion of metals and calcareous stones. Mar Chem. 1990;30:113–22. https://doi.org/10.1016/0304-4203(90)90065-K.
7. Scrano L, Laviano R, Eramo G, Salvi AM, Santacroce M, Cardellicchio F, Bufo SA. Extensive preventive diagnostics for biocleaning and bio-consolidation of two rupestrian churches. XXVIII Congress of the Analytical Chemistry Division, Bari, Italy, September 2019, Book of Abstracts, ISBN: 978–88–94952–10–0
8. Salvi AM, Langerame F, Macchia A, Sammartino MP, Tabasso ML. XPS characterization of (copper-based) coloured stains formed on limestone surfaces of outdoor Roman monuments. Chem Cent J. 2012. https://doi.org/10.1186/1752-153X-6-S2-S10.
9. Macchia A, Tabasso ML, Salvi AM, Sammartino MP, Mangialardo S, Dore P, Postorino P. Analytical characterization of corrosion products of copper and its alloys on stained stone surfaces. Surf Interface Anal. 2013;45(7):1073–80. https://doi.org/10.1002/sia.5220.
10. Macchia A, Ruffolo SA, Rivaroli L, La Russa MF. The treatment of iron-stained marble: toward a"green" solution". Int J Conserv Sci. 2016;7:323–32.
11. Spile S, Suzuki T, Bendix J, Simonsen KP. Effective cleaning of rust stained marble. Herit Sci. 2016;4(1):1–10. https://doi.org/10.1186/s40494-016-0081-6.
12. Langerame F, Lovaglio T, Reale R, Salvi AM, Sammartino MP, Visco G. Iron stains on carbonatic stones: XPS investigation on corrosion–induced deterioration. SCI 2016 - ISA Biennial Meeting, Matera (Italy). Abstract Book: 54–55. http://hdl.handle.net/11563/124937
13. Reale R, Campanella L, Sammartino MP, Visco G, Bretti G, Ceseri M, Natalini R, Notarnicola F. A mathematical and experimental study on iron rings formation in porous stones. J Cult Herit. 2019;38:158–66. https://doi.org/10.1016/j.culher.2019.01.012.
14. Reale R. Chromatic alterations of carbonate stone materials: study of stains induced by coexistence with ferrous materials and innovative methods for their removal. PhD thesis 2017: 227 pp. https://iris.uniroma1.it/handle/11573/1022194#.YYbSZ2DMKUk
15. Cornell RM, Schwertmann U. The iron oxides: structure, properties, reactions, occurrences and uses. New York: John Wiley & Sons; 2003. https://doi.org/10.1002/3527602097.
16. Stambolov T, Van Rheeden B. Note on the removal of rust from old iron with thioglycolic acid. Stud Conserv. 1968;13(3):142–4. https://doi.org/10.2307/1505318.
17. Gervais C, Grissom CA, Little N, Wachowiak MJ. Cleaning marble with ammonium citrate. Stud Conserv. 2010;55(3):164–76. https://doi.org/10.1179/sic.2010.55.3.164.
18. Thorn A. Treatment of heavily iron-stained limestone and marble sculpture. In: Verger I, James J, editors. ICOM Committee for Conservation 14th Triennial Meeting. Copenhagen: ICOM Publications; 2005. p. 888–94.
19. Rueda EH, Ballesteros MJ, Grassi RL. Dithionite as a dissolving reagent for goethite in the presence of EDTA and citrate. Application to soil analysis. Clays and Clay Miner. 1992;40(5):575–85.
20. New Jersey Department of Health and Senior Service. Hadarzous Substance Fact Sheet: Thioglycolic acid, 2015: 6 pp. https://www.nj.gov/health/eoh/rtkweb/documents/fs/1848.pdf
21. Igawa M, Kanamori H, Nanzai B. Gel-phase extraction for the removal of heavy metal ions. Chem Lett. 2010;39(9):996–7. https://doi.org/10.1246/cl.2010.996.
22. Sansonetti A, Bertasa M, Canevali C, Rabbolini A, Anzani M, Scalarone D. A review in using agar gels for cleaning art surfaces. J Cult Herit. 2020;44:285–96. https://doi.org/10.1016/j.culher.2020.01.008.
23. Hatcher HC, Singh RN, Torti FM, Torti SV. Synthetic and natural iron chelators: therapeutic potential and clinical use. Future Med Chem. 2009;1(9):1643–70. https://doi.org/10.4155/fmc.09.121.
24. Khalaf RW. A viewpoint on the reconstruction of destroyed UNESCO Cultural World Heritage Sites. Int J Herit Stud. 2017;23(3):261–74. https://doi.org/10.1080/13527258.2016.1269239.
25. Aasa R, Malmström B, Saltman P, Vänngård T. The specific binding of iron (III) and copper (II) to transferrin and conalbumin. Biochem Biophys Acta. 1963;75:203–22. https://doi.org/10.1016/0006-3002(63)90599-7.
26. Hirose M. The structural mechanism for iron uptake and release by transferrins. Biosci Biotechnol Biochem. 2000;64(7):1328–36. https://doi.org/10.1271/bbb.64.1328.
27. Abdallah FB, Chahine JMEH. Transferrins: iron release from lactoferrin. J Mol Biol. 2000;303(2):255–66. https://doi.org/10.1006/jmbi.2000.4101.
28. Giansanti F, Leboffe L, Angelucci F, Antonini G. The nutraceutical properties of ovotransferrin and its potential utilization as a functional food. Nutrients. 2015;7(11):9105–15. https://doi.org/10.3390/nu7115453.
29. Giansanti F, Leboffe L, Pitari G, Ippoliti R, Antonini G. Physiological roles of ovotransferrin. Biochimica et Biophysica Acta (BBA) General Subjects. 2012;1820(3):218–25. https://doi.org/10.1016/j.bbagen.2011.08.004.
30. Parkar DR, Jadhav RN, Pimpliskar MR. Extraction and characterization of lactoferrin from commercial milk. Int J Pharm Pharm Res. 2016;6(2):355–61.
31. Wu J, Acero-Lopez A. Ovotransferrin: structure, bioactivities, and preparation. Food Res Int. 2012;46(2):480–7. https://doi.org/10.1016/j.foodres.2011.07.012.
32. Abeyrathne EDNS, Lee HY, Ham JS, Ahn DU. Separation of ovotransferrin from chicken egg white without using organic solvents. Poult Sci. 2013;92(4):1091–7. https://doi.org/10.3382/ps.2012-02654.
33. Sassoni E, Franzoni E. Influence of porosity on artificial deterioration of marble and limestone by heating. Mater Sci Process. 2014;115:809–16. https://doi.org/10.1007/s00339-013-7863-4.
34. Amoroso GG, Camaiti M. Scienza dei materiali e restauro, la pietra: dalle mani degli artisti e degli scalpellini a quelle dei chimici macromolecolari. Alinea Ed. 1997; 320 pp.
35. Vergès-Belmin V, Heritage A, Bourgès A. Powdered cellulose poultices in stone and wall painting conservation-myths and realities. Stud Conserv. 2011;56(4):281–97. https://doi.org/10.1179/204705811X13159282692923.
36. Bosch-Roig P, Lustrato G, Zanardini E, Ranalli G. Biocleaning of Cultural Heritage stone surfaces and frescoes: which delivery system can be the most appropriate? Ann Microbiol. 2015;65:1227–41. https://doi.org/10.1007/s13213-014-0938-4.

37. UNI EN ISO 11664–2 Part 2: CIE standard illuminants, International Organization for Standardization Publisher: 2007.
38. Schneider CA, Rasband WS, Eliceiri KW. NIH Image to ImageJ: 25 years of image analysis. Nature Methods 2012;9(7):671–75. https://doi.org/10.1038/nmeth.2089.
39. Berns R, Taplin L, Nezamabadi M. Spectral imaging using a commercial colour-filter array digital camera. Published in the 14th Triennial Meeting the Hague Preprints. 2005. 2: 743–750. http://scholarworks.rit.edu/article.
40. Torrent J, Barrón V. Diffuse reflectance spectroscopy of iron oxides. In: Hubbard Arthur T, editor. Encyclopedia of surface and colloid science. Boca Raton: CRC Press; 2002. p. 1438–46.
41. Yang L, Kruse B. Revised Kubelka-Munk theory.I. Theory and application. J Opt Soc Am. 2004;21(10):1933–41. https://doi.org/10.1364/JOSAA.21.001933.
42. Scheinost AC, Chavernas A, Barrón V, Torrent J. Use and limitations of second-derivative diffuse reflectance spectroscopy in the visible to near-infrared range to identify and quantify Fe oxide minerals in soils. Clays Clay Miner. 1998;46(5):528–36. https://doi.org/10.1346/CCMN.1998.0460506.
43. Castle JE, Salvi AM. Chemical state information from the near-peak region of the X-ray photoelectron background. J Electron Spectrosc Relat Phenom. 2001;114–116:1103–13. https://doi.org/10.1016/S0368-2048(00)00305-4.
44. Castle JE, Chapman-Kpodo H, Proctor A, Salvi AM. Curve-fitting in XPS using extrinsic and intrinsic background structure. J Electron Spectrosc Relat Phenom. 2000;106(1):65–80. https://doi.org/10.1016/S0368-2048(99)00089-4.
45. Briggs D, Grant JT. Surface analysis by Auger and X-ray photoelectron spectroscopy. Chichester: IM Publications and Surface Spectra limited; 2003. p. 345–75.
46. NIST: National Institute of Standards and Technology. X-ray Photoelectron Spectroscopy Database, version 4.1, 2012. https://doi.org/10.18434/T4T88K.
47. Simmons EL. Relation of diffuse reflectance remission function to the fundamental optical parameters. Optical Acta. 1972;19:845–51. https://doi.org/10.1080/713818505.
48. Sherman DM, Waite TD. Electronic spectra of Fe^{3+} oxides and oxide hydroxides in the near IR to near UV. Am Miner. 1985;70:1262–9.
49. Tsai F, Philpot W. Derivative analysis of hyperspectral data. Rem Sens Environ. 1998;66:41–51. https://doi.org/10.1117/12.262471.
50. Graat PCJ, Somers MAJ. Simultaneous determination of composition and thickness of thin iron oxide films from XPS Fe2p spectra. Appl Surf Sci. 1996;100–101:36–40. https://doi.org/10.1016/0169-4332(96)00252-8.
51. Beamson G, Briggs D. High resolution XPS of organic polymers the Scienta ESCA 300 Database. Chichester: Wiley; 1992. https://doi.org/10.1002/adma.19930051035.
52. Carbone ME, Ciriello R, Guerrieri A, Salvi AM. Poly(o-aminophenol) electrosynthesized onto platinum at acidic and neutral pH: comparative investigation on the polymers characteristics and on their inner and outer interfaces. Int J Electrochem Sci. 2014;9:2047–66.
53. Alessandrini G, Toniolo L, Cariati F, Daminelli G, Polesello S, Pozzi A. A black paint on the facade of a renaissance building in Bergamo Italy. Stud Conserv. 2013;41(4):193–204. https://doi.org/10.1179/sic.1996.41.4.193.
54. Garcia-Vallès M, Vendrell-Saz M, Molera J, Blazquez F. Interaction of rock and atmosphere: patinas on Mediterranean monuments. Environ Geol. 1998;36:137–49. https://doi.org/10.1007/s002540050329.
55. Polo A, Cappitelli F, Brusetti L, Principi P, Villa F, Giacomucci L, Ranalli G, Sorlini C. Feasibility of removing surface deposits on stone using biological and chemical remediation methods. Microb Ecol. 2010;60:1–14. https://doi.org/10.1007/s00248-009-9633-6.
56. Vindedahl AM, Strehlau JH, Arnold WA, Penn RL. Organic matter and iron oxide nanoparticles: aggregation, interactions, and reactivity. Environ Sci Nano. 2016;3:494–505. https://doi.org/10.1039/C5EN00215J.
57. Yamamoto T, Juneja LR, Hatta H, Kim M. Hen eggs, their basic and applied science. Boca Raton: CRC Press; 1996. https://doi.org/10.1201/9780203752081.
58. Campanella L, Dell'Aglio E, Reale R, Cardellicchio F, Salvi AM, Casieri C, Cerichelli G, Gabriele F, Spreti N, Bernardo G, Guida A, Porcari V. Development of natural gels for cleaning the stone materials of cultural heritage from iron stains and biodeteriogenic microorganisms. Proceedings of XII International Conference Diagnosis, Conservation and Enhancement of the Cultural Heritage. Naples 9–10 December 2021: 313–324. ISBN 978 88 95609 61 4
59. Bernardo G, Guida A, Porcari V, Campanella L, Dell'Aglio E, Reale R, Cardellicchio F, Salvi A.M, Casieri C, Cerichelli G, Gabriele F, Spreti N. New materials and diagnostic techniques to prevent and control calcarenite degradation. Proceedings of XII International Conference Diagnosis, Conservation and Enhancement of the Cultural Heritage. Naples 9–10 December 2021: 325–334. ISBN 978 88 95609 61 4
60. Giansanti F, Panella G, Leboffe L, Antonini G. Lactoferrinfrom milk: nutraceutical and pharmacological properties. Pharmaceuticals (Basel). 2016;9(4):61. https://doi.org/10.3390/ph9040061.
61. Superti F, Ammendolia MG, Berlutti F, Valenti P. Ovotransferrin. In: Huopalahti R, López-Fandiño R, Anton M, Schade R, editors. Bioactive Egg Compounds. Heidelberg: Springer; 2007.

Publisher's Note